IEEE Access
Multidisciplinary ⋮ Rapid Review ⋮ Open Access Journal

Received February 11, 2020, accepted March 15, 2020, date of publication April 8, 2020, date of current version April 30, 2020.

Digital Object Identifier 10.1109/ACCESS.2020.2986516

Analysis of Electromagnetic Interference Between Open Cable Trays

JAEYUL CHOO[1], HOON-KEUN LEE[2], JONG-EON PARK[3], HOSUNG CHOO[4], AND YONG-HWA KIM[5]

[1]Department of Instrumentation, Control, and Electrical System, Korea Institute of Nuclear Safety, Daejeon 34142, South Korea
[2]Department of Safety Research, Korea Institute of Nuclear Safety, Daejeon 34142, South Korea
[3]Department of Safety Engineering, Dongguk University, Gyeongju 38066, South Korea
[4]School of Electronic and Electrical Engineering, Hongik University, Seoul 04066, South Korea
[5]Department of Electronic Engineering, Myongji University, Yongin 17058, South Korea

Corresponding author: Yong-Hwa Kim (yongkim@mju.ac.kr)

This work was supported in part by the Nuclear Safety Research Program through the Korea Foundation of Nuclear Safety (KoFONS) granted Financial Resource from the Nuclear Safety and Security Commission (NSSC) of South Korea under Grant 1805006, in part by the National Research Foundation of Korea (NRF) grant funded by the Korean Government (MSIT) under Grant 2019R1A2C2086621, and in part by the Basic Science Research Program through the National Research Foundation of Korea (NRF) funded by the Ministry of Education under Grant 2015R1A6A1A03031833.

ABSTRACT This paper presents an analytical interpretation of electromagnetic interference between solid-bottom type open cable trays in a nuclear power plant under the assumption that an electric-line current is undesirably generated from a damaged cable in an open cable tray. Based on the superposition principle and Helmholtz's equation in conjunction with the separation of variables, we employ a mode-matching method to obtain analytical solutions to the postulated electromagnetic interference problem. Before conducting a mode-matching analysis, we investigate the radiating principle of the electric field interfering with a victim cable tray by deriving the array factor in consideration of an imaginary electric-line current. In addition, we characterize the electric fields with a propagating mode at an observation point in the victim cable tray using the derived expression of the electric field. Based on this, we validate the formulation and computation of our mode-matching method and then computationally investigate the strength and distribution of interfering electric fields in terms of the separation distances provided in regulatory guidance on the electrical independence of a nuclear power plant. Finally, we compute the strength and distribution of the interfering electric field at the observation point when the location of an electric-line current is modified. The results of the study provide us with the useful information to alleviate the electromagnetic interference between open cable trays in a nuclear power plant.

INDEX TERMS Electromagnetic interference, mode-matching method, open cable tray.

I. INTRODUCTION

Cable trays have been employed to protect and isolate power and communication cables from physical, electromagnetic (EM), and fire damage in industrial facilities such as nuclear power plants. In terms of their cover, cable trays are categorized into open-type cable trays such as the solid-bottom type and enclosed-type cable trays such as the box-type. While an open-type cable tray has the advantages of low fabrication costs and structural simplicity, it inevitably retains its vulnerability to external damage such as EM interference (EMI); this may deteriorate the integrity of the power and signal transmitted through the cable tray [1].

In view of electromagnetics, many studies have been conducted on cable trays [2]–[10]. Reference [2] reported the shielding effectiveness of a cable tray with various magnetic and electric materials against inductive and capacitive proximity-coupling. The performance of EM protection of open cable trays with various shapes was studied in [3]. Furthermore, the mutual EM coupling between cables in enclosed and open trays was analyzed in [4], [5]. The transfer impedance of a U-shaped enclosed cable tray and an open cable tray of various shapes was studied using conformal transformation in [6]–[8]. The transfer impedance of an

The associate editor coordinating the review of this manuscript and approving it for publication was Mehmet Alper Uslu.

enclosed cable tray in terms of the ratio of width to height as well as the connecting scheme between cable trays was reported in [9], [10]. However, there are few studies that analyze the EM coupling between cable trays that leads to EMI problems.

Thus, in this study, we conduct a mode-matching analysis on the EMI between open cable trays in a nuclear power plant. We then compare the analyzed EMI with the allowable EMI levels derived from the regulatory guidance associated with EMI in nuclear power plants. Here, we consider that the open cable trays, which are placed parallel to each other, are infinitely extended with a constant separation distance in an indoor environment of a nuclear power plant. To express an EMI source, we assume that an undesired electric-line current is generated by a damaged cable in an open cable tray.

The rest of the paper is organized as follows. In Section II, we provide a summary of the regulatory requirements for nuclear power plants; cable trays are required to be separated at certain distances depending on their placement, and allowable levels of EMI are provided corresponding to the required separation distances. In Section III, we explain the analyzed model, formulate the EM fields, enforce the boundary conditions, and calculate a set of simultaneous equations for our mode-matching analysis. In Section IV, we derive an approximate interpretation of the radiating field of an electric-line current and the coupled field at an observation point in the victim cable tray. In Section V, we investigate the electric-field distributions by varying either the separation distance, the configuration of cable trays, or the location of the electric-line current. In Section VI, we conclude that the results of our study provide useful information for the electromagnetically robust installation of open cable trays.

II. REGULATORY GUIDANCE ON ELECTRICAL INDEPENDENCE AND ELECTROMAGNETIC INTERFERENCE

The instrumentation and control (I&C) equipment of nuclear power plants has recently been upgraded from analog to digital systems. While the digitalization of I&C equipment provides several advantages, such as low fabrication cost, owing to simple designs, it simultaneously requires precautions to be undertaken against possible EMI problems. Thus, the United States Nuclear Regulatory Commission (U.S. NRC) published Regulatory Guide (Reg. Guide) 1.180 that provides regulatory guidance pertaining to the categories, methods, and allowable interference levels and susceptibility threshold levels for electromagnetic compatibility (EMC) tests [11]. In addition, Reg. Guide 1.75 effectively endorses IEEE Std. 384, which describes the process of realizing independence of electric equipment and circuits for safety functions in highly disturbed environments with EMI, missiles, combustible material, flooding, etc., [12]. Herein, based on the aforementioned regulatory guidance, we describe the minimum separation distance required between cable trays to ensure independence. We then derive the allowable levels of EMI corresponding to the minimum separation distances required between open cable trays that are parallel to each other.

A. REGULATORY GUIDANCE ON INDEPENDENCE

Circuits and electrical equipment related to safety functions in a nuclear power plant are required to be independent to ensure safety against existing potential hazards such as fires and EMI. Specifically, Reg. Guide 1.75 describes an acceptable method for complying with the regulation with respect to the physical independence requirements of circuits and electrical equipment that comprise or are associated with safety systems. Reg. Guide 1.75 adopts IEEE Std. 384 that describes specific criteria for physical separation and electrical isolation of circuits and electrical equipment to meet this independence requirement [13].

Regarding the separation between cable trays, IEEE Std. 384 requires a minimum separation distance (D_{min}) as a precaution against potential thermal hazards. Fig. 1 shows the categorized configurations determined by the combination of open and enclosed cable trays, as well as the horizontal and vertical separation distances (D) corresponding to each configuration. Similarly, Table 1 represents D_{min}, in the limited hazard area, which is demonstrated in [13], corresponding to the vertical and horizontal interactions in terms of the placement of open and enclosed cable trays in Fig. 1. From Table 1, we can observe that D_{min} in an open-to-open configuration increases if either the size of the contained cable or the voltage

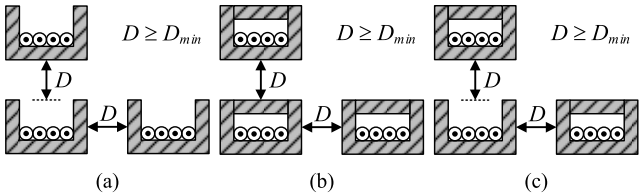

FIGURE 1. Configurations in terms of combination of open and enclosed cable trays. (a) Open-to-open, (b) enclosed-to-enclosed, (c) enclosed-to-open configurations.

TABLE 1. Minimum separation distances for limited hazard areas.

Configuration	Interactions		
	Involving I&C cables only(1)	Involving low-voltage power circuits with cable size ≤ 2/0 AWG	Involving low-voltage power circuits with cable size > 2/0 AWG and all medium-voltage power circuit
Open-to-open	H(2): 25 mm V(2): 76 mm	H: 152 mm V: 305 mm	H: 920 mm V: 1530 mm
Enclosed-to-enclosed	H: 25 mm V: 25 mm	H: 25 mm V: 25 mm	H: 25 mm V: 25 mm
Enclose-to-open	H: 25 mm V: 76 mm(3)	H: 152 mm V: 305 mm(3), (4)	H: 920 mm V: 1530 mm(3), (4)

(1) The minimum separation distances are the same as those for nonhazard areas.
(2) H and V indicate horizontal and vertical D_{min}, respectively.
(3) Vertical separation may be reduced to 25 mm if the enclosed tray is below the open tray.
(4) The minimum separation may be reduced to 25 mm horizontal and 76 mm vertical if the circuits in the open configuration are limited to I&C circuits.

of power circuits increases. An enclosed-to-enclosed configuration is interesting in that the both vertical and horizontal separation distances require a minimum constant distance of 25 mm ($D_{min} = 25$ mm) because enclosed cable trays can effectively shield and isolate the inner cables from external influences. However, IEEE Std. 384 states that the minimum separation distances in Table 1 are based on thermal effects of internal failures or faults in electrical equipment or cables and do not consider EMI. Therefore, IEEE Std. 384 recommends conducting an EM analysis or testing the electrical equipment including cable trays to establish an acceptable separation distance to address EMI. Thus, herein, we interpret the EM interaction in open-to-open configurations (cases where the horizontal D_{min} is 25 mm, 152 mm, and 920 mm) under the assumption that an enclosed cable tray can perfectly shield and isolate cables.

B. REGULATORY GUIDANCE ON ELECTROMAGNETIC INTERFERENCE AND SUSCEPTIBILITY BY RADIATION

Reg. Guide 1.180 provides information on the methodologies, criteria for acceptance, and alternative tests for EMC, based on EMI and electromagnetic susceptibility (EMS) tests. Based on Reg. Guide 1.180, EMC tests should be accomplished using the method of the endorsed military standard [14]; the EMC test results must comply with the acceptance criteria to ensure safety of the nuclear power plant. In particular, for the radiating EMI between cable trays, Reg. Guide 1.180 provides a method to evaluate the EMI and EMS by a radiating electric field (E-field) at a distance of 1 m from target equipment, such as cable trays, in the form of RE102 and RS103 tests, respectively. In detail, the RE102 test aims to evaluate the amount of undesired electric field radiated by the equipment under test (EUT); the RS103 test aims to evaluate how well the functional integrity of the EUT is maintained against external interference of electric fields.

Fig. 2 shows the allowable strength of a radiating electric field in an RE102 test and the susceptibility threshold level (10 V/m = 140 dBμV/m) against an interfering electric field in an RS103 test, as illustrated by the black and pink lines, respectively. Accordingly, satisfying the acceptance criterion of the RS103 test ensures that the EUT can function without any degradation during exposure to an interfering electric field lower than 10 V/m. In other words, this implies that other equipment close to the equipment qualified by the RS103 test should not emit an electric field stronger than 10 V/m at a separation distance of 1 m, as shown in Fig. 2. Thus, to limit the strength of the interfering electric-field radiated from the adjacent equipment to the acceptable strength considered using the margin from the susceptibility threshold level of 10 V/m, the RE102 test requires the EUT to radiate electric fields lower than the allowable strength at a distance of 1 m, as illustrated by the black line in Fig. 2. In addition, we derive the allowable strength of the interfering electric field at distances of 25, 152, and 920 mm, which are the horizontal minimum separation distances (D_{min}) corresponding to open-to-open configurations listed in Table 1; these are

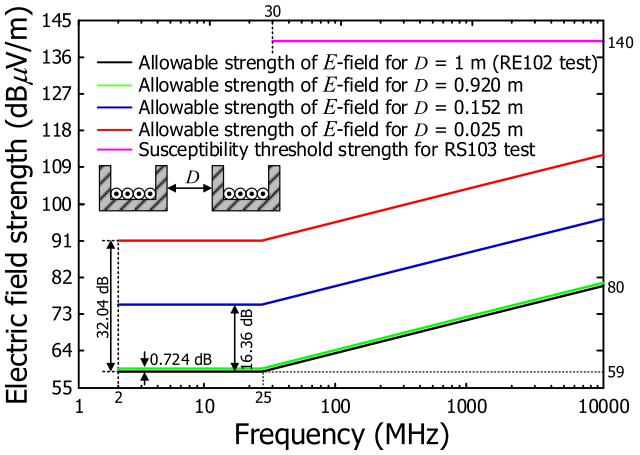

FIGURE 2. Allowable E-field strength for RE102 test, modified allowable E-field strengths at distances of 0.025, 0.152, and 0.92 m, and susceptibility threshold level for RS103 test.

illustrated by the red, blue, and green lines in Fig. 2. In this derivation, we assume that the radiating electric field propagates in the far-field region where the electric-field strength decreases inversely with the propagating distance (E-field strength $\propto 1 / D$).

III. MODE-MATCHING FORMULATION

Based on the regulatory guidance on electrical independence and EMI, we examine the EMI between open cable trays by employing a mode-matching method. This method is selected as it enables us to interpret the EM problem in terms an individual mode, as well as efficiently derive the EM characteristics owing to the rapid convergence of the series solution. The mode-matching analysis is conducted in the following order: separation of the overall analyzed region, representation of EM fields using Helmholtz's equation in conjunction with separation of variables, and enforcement of boundary conditions on the tangential-field continuities between the separated regions. In particular, we employ the superposition principle to express an electric-line current in the cable tray as an EMI source. In this section, we introduce the modeling of open cable trays in an indoor environment and describe the aforementioned mode-matching formulation in detail.

A. CONFIGURATIONS OF OPEN CABLE TRAYS

Fig. 3 shows the various classifications of open cable trays. Ladder-type, perforated-type, and solid-bottom type cable trays can be applied when installing power cables of a large size and power, medium-sized I&C cables, and small-sized I&C cables, respectively.

Solid-bottom type open cable trays are particularly suitable for protecting I&C cables from external EM compared to other types of cable trays. However, shielding covers are sometimes required for enclosed cable trays to realize a better shielding performance against EMI; installing such covers requires high cost. Therefore, estimating the EMI between

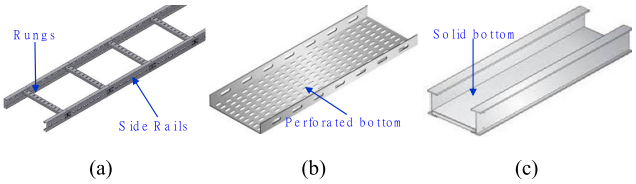

FIGURE 3. Classification of cable trays (a) ladder-type (b) perforated-type, (c) solid-bottom type.

open cable trays through an EM analysis can aid in deciding whether a shielding cover should be applied. With this as our motivation, we analyze the EMI between open cable trays of a solid-bottom type in an indoor environment of a nuclear power plant.

We establish a simple model of two open cable trays of the solid-bottom type in a nuclear power plant as shown in Fig. 4, where we assume that the open cable trays are infinitely long along the y-axis.

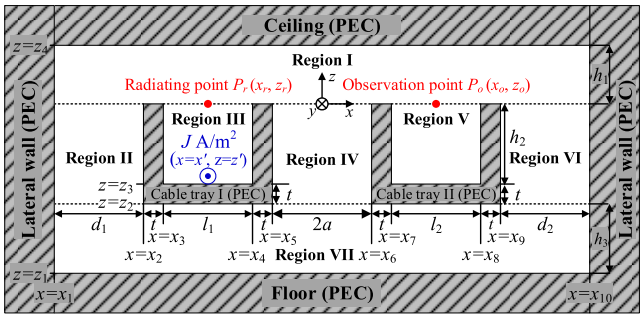

FIGURE 4. Configuration of two open cable trays in an indoor environment of a nuclear power plant.

In Fig. 4, the cable tray I (thickness t and internal size $l_1 \times h_2$) and cable tray II (thickness t and internal size $l_2 \times h_2$) are separated by a distance of $2a$ (separation distance $D = 2a$) and are located at distances of h_1, h_3, d_1, and d_2 from the ceiling, floor, and two lateral walls, respectively. We assume that an electric-line current (strength J) of a damaged cable generates an EM field as the EMI at ($x = x'$, $z = z'$) and the materials of the cable trays, ceiling, floor, lateral walls are perfect electric conductors (PECs). To formulate the EM fields, we divide the overall region in free space in Fig. 4 into seven subregions (regions I–VII). To quantitatively evaluate the EMI from cable tray I to cable tray II, we define the radiating point P_r ($x = x_r$, $z = z_r$) and the observation point P_o ($x = x_o$, $z = z_o$) as the center of the open surfaces ($z = 0$) of both cable trays I and II, respectively, as depicted in Fig. 4.

B. FIELD REPRESENTATION

We employ the superposition principle to represent the EM fields; we consider two individual cases: with an electric-line current in open cable tray I and without an electric-line current in cable tray I enclosed (covered) by the PEC. For the case where the electric-line current exists at ($x = x'$, $z = z'$), we only consider region III owing to the PEC cover, which results in an incident electric field as follows [15]−[17].

$$E_y^i(x,z) = \begin{cases} \sum_{m_3=1}^{M_3} J\chi_{m_3}(x',x)v_{m_3}(z',z), & z' < z \le 0 \\ \sum_{m_3=1}^{M_3} J\chi_{m_3}(x',x)v_{m_3}(z,z'), & -h_2 \le z < z' \end{cases} \quad (1)$$

where $v_{m_3}(\alpha, \beta) = \sin\xi_{m_3}(\alpha - z_3)\sin\xi_{m_3}\beta$ and $\chi_{m_3}(\alpha, \beta) = -2i\omega\mu_3 \sin\gamma_{m_3}(\alpha - x_3)\sin\gamma_{m_3}(\beta - x_3) / (l_1\xi_{m_3}\sin\xi_{m_3}h_2)$. Herein, $\gamma_{m_3} = m_3\pi / (x_4 - x_3)$, $\xi_{m_3} = \sqrt{k^2 - \gamma_{m_3}^2}$, and M_3 is the maximum mode number in region III.

For the other case where there is no electric-line current, we derive the expressions of electric fields in regions I−VII based on the Helmholtz equation in conjunction with the separation of variables, as follows [15].

$$E_y^I(x,z) = i\omega \sum_{m_1=1}^{M_1} A_{m_1} \sin\gamma_{m_1}(x - x_1)\sin\xi_{m_1}(z - z_4) \quad (2)$$

$$E_y^{II}(x,z) = i\omega \sum_{m_2=1}^{M_2} \sin\gamma_{m_2}(x - x_1) \times (A_{m_2}\sin\xi_{m_2}z + B_{m_2}\cos\xi_{m_2}z) \quad (3)$$

$$E_y^{III}(x,z) = i\omega \sum_{m_3=1}^{M_3} A_{m_3} \sin\gamma_{m_3}(x - x_3)\sin\xi_{m_3}(z - z_3) \quad (4)$$

$$E_y^{IV}(x,z) = i\omega \sum_{m_4=1}^{M_4} \sin\gamma_{m_4}(x - x_5) \times (A_{m_4}\sin\xi_{m_4}z + B_{m_4}\cos\xi_{m_4}z) \quad (5)$$

$$E_y^{V}(x,z) = i\omega \sum_{m_5=1}^{M_5} A_{m_5} \sin\gamma_{m_5}(x - x_7)\sin\xi_{m_5}(z - z_3) \quad (6)$$

$$E_y^{VI}(x,z) = i\omega \sum_{m_6=1}^{M_6} \sin\gamma_{m_6}(x - x_9) \times (A_{m_6}\sin\xi_{m_6}z + B_{m_6}\cos\xi_{m_6}z) \quad (7)$$

$$E_y^{VII}(x,z) = i\omega \sum_{m_7=1}^{M_7} A_{m_7} \sin\gamma_{m_7}(x - x_1)\sin\xi_{m_7}(z - z_1) \quad (8)$$

where M_1, M_2, M_3, M_4, M_5, M_6, and M_7 are the maximum mode numbers, $\gamma_{m_1} = m_1\pi/(x_{10} - x_1)$, $\gamma_{m_2} = m_2\pi / (x_2 - x_1)$, $\gamma_{m_4} = m_4\pi / (x_6 - x_5)$, $\gamma_{m_5} = m_5\pi / (x_8 - x_7)$, $\gamma_{m_6} = m_6\pi / (x_{10} - x_9)$, $\gamma_{m_7} = m_7\pi / (x_{10} - x_1)$, $\xi_{m_1} = \sqrt{k^2 - \gamma_{m_1}^2}$, $\xi_{m_2} = \sqrt{k^2 - \gamma_{m_2}^2}$, $\xi_{m_4} = \sqrt{k^2 - \gamma_{m_4}^2}$, $\xi_{m_5} = \sqrt{k^2 - \gamma_{m_5}^2}$, $\xi_{m_6} = \sqrt{k^2 - \gamma_{m_6}^2}$, $\xi_{m_7} = \sqrt{k^2 - \gamma_{m_7}^2}$.

Note that the representation of the magnetic field (H_x) in each region can be derived by applying the relationship of $H_x = (i/\omega\mu)\cdot(dE_y/dz)$ to (1)−(8).

C. ENFORCEMENT OF BOUNDARY CONDITIONS

The unknown modal coefficients A_{m_1}, A_{m_2}, A_{m_3}, A_{m_4}, A_{m_5}, A_{m_6}, A_{m_7}, B_{m_2}, B_{m_4}, and B_{m_6} in (2)−(8) can be determined by enforcing the boundary conditions on the continuities of the tangential electric and magnetic fields (E_y and H_x) at $z = 0$ and $z = z_2$. The continuities of the tangential electric and magnetic fields at $z = 0$ are expressed as follows.

$$E_y^I(x,z)\Big|_{z=0} = \begin{cases} E_y^{II}(x,z)\Big|_{z=0} & , \ x_1 \le x < x_2 \\ 0 & , \ x_2 \le x < x_3 \\ E_y^i(x,z)\Big|_{z=0} + E_y^{III}(x,z)\Big|_{z=0} & , \ x_3 \le x < x_4 \\ 0 & , \ x_4 \le x < x_5 \\ E_y^{IV}(x,z)\Big|_{z=0} & , \ x_5 \le x < x_6 \\ 0 & , \ x_6 \le x < x_7 \\ E_y^{V}(x,z)\Big|_{z=0} & , \ x_7 \le x < x_8 \\ 0 & , \ x_8 \le x < x_9 \\ E_y^{VI}(x,z)\Big|_{z=0} & , \ x_9 \le x < x_{10} \end{cases} \quad (9)$$

$$H_x^I(x,z)\Big|_{z=0} = H_x^{II}(x,z)\Big|_{z=0} \quad , \ x_1 < x < x_2 \quad (10)$$

$$H_x^I(x,z)\Big|_{z=0} = H_x^i(x,z)\Big|_{z=0} + H_x^{III}(x,z)\Big|_{z=0} \quad , \ x_3 < x < x_4 \quad (11)$$

$$H_x^I(x,z)\Big|_{z=0} = H_x^{IV}(x,z)\Big|_{z=0} \quad , \ x_5 < x < x_6 \quad (12)$$

$$H_x^I(x,z)\Big|_{z=0} = H_x^{V}(x,z)\Big|_{z=0} \quad , \ x_7 < x < x_8 \quad (13)$$

$$H_x^I(x,z)\Big|_{z=0} = H_x^{VI}(x,z)\Big|_{z=0} \quad , \ x_9 < x < x_{10} \quad (14)$$

The boundary conditions on the continuities of the tangential electric and magnetic fields at $z = z_2$ are analogous to (9)–(14). The results from the enforcement of the boundary conditions constitute a set of simultaneous equations to determine the unknown modal coefficients. Note that the specific procedure to build a set of simultaneous equations from enforcing the boundary condition is similarly presented in [17], [18]. In the Appendix, we append the boundary conditions at $z = z_2$, and describe the simultaneous equations derived from boundary conditions using a matrix equation.

IV. APPROXIMATE ESTIMATION OF EM FIELDS OF CABLE TRAYS

Electric-field distributions in cable trays I and II (regions III and V) are governed by (1), (4), and (6). This implies that geometrical parameters, such as the lengths of the bottom plates of cable trays I and II, as well as the location of the electric-line current, are important factors when determining the electric-field distributions. Before accounting for specific mode-matching formulation and computation, we approximately estimate the electric fields in cable trays I and II by using image theory and performing a modal analysis mathematically, respectively.

A. APPROXIMATE EVALUATION OF E-FIELD RADIATED FROM CABLE TRAY I

First, we approximately derive an electric-field characteristic in terms of the distance between the central electric-line current and the bottom plate of cable tray I. We consider a virtual (imaginary) electric-line current with the opposite phase using image theory under the assumption that the bottom plate (PEC) with a negligible thickness functions as an extended ground plane [19], [20].

Fig. 5 shows the results of applying an imaginary electric-line current to cable tray I when the bottom plate functions as an extended ground plane as the ratio $T(= h_2 / l_1)$ approaches zero (l_1 is considerably greater than h_2). Then, we approximately estimate the radiating characteristic of the electric field by obtaining an array factor under the condition that only the original and imaginary electric-line currents exist in the free space [21]. The resulting array factor AF corresponding to the result shown in Fig. 5 is derived as (15). From (15), we can establish that the distance c in Fig. 5 is the dominant factor when determining AF in the observation direction ($\psi = \psi_o$).

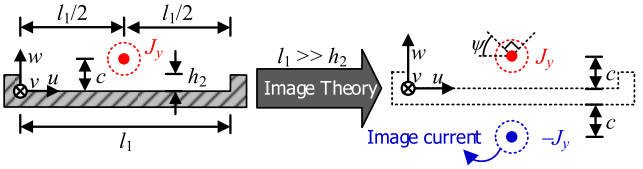

FIGURE 5. Application of image theory to derive the radiating characteristic of cable tray I when the ratio T ($= h_2 / l_1$) approaches zero.

In particular, the array factor AF in the observation direction of $\psi = \pi/2$ (in front of the aperture surface of cable tray I) can be expressed as (16). Through (16), we can establish that the magnitude of AF is maximum when the distance c between the electric-line current and the bottom plate of cable tray I in Fig. 5 is $(2n - 1)\lambda/4$ (n: positive integer and λ: wavelength). Note that the radiating principle considered in this analysis is similar to the operating principle of a reflector backed antenna; furthermore, it is practical to use when making an approximate prediction of the radiating electric field [20].

$$AF(c, \psi) = -2iJ_y \sin\left(\frac{2\pi}{\lambda} c \sin\psi\right) \quad (15)$$

$$AF(c, \psi = \frac{\pi}{2}) = -2iJ_y \sin\frac{2\pi}{\lambda} c \quad (16)$$

B. ANALYSIS OF EMI WITH CABLE TRAY II

Second, we investigate the electric-field characteristics at the observation point P_o ($x = x_o$, $z = z_o$) in cable tray II by employing a general model as illustrated in Fig. 6.

In Fig. 6, the total internal length (L) is determined by summing the length of the bottom plate ($\alpha\lambda$) and the lengths of the lateral walls ($\beta\lambda$) ($L = \alpha\lambda + 2\beta\lambda$). In addition, we define the ratio T as the ratio of the length of the bottom plate to the length of the side wall ($T = \beta\lambda/\alpha\lambda = \beta/\alpha$).

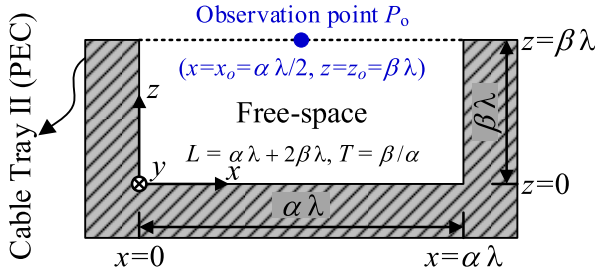

FIGURE 6. General model of cable tray II including observation point Po (xo, zo).

Based on the two-dimensional Helmholtz equation, the electric field (E_y) in cable tray II is expressed by a combination of the electric fields propagating in the $+z$ and $-z$ directions, as expressed in (17). The electric field at observation point P_o ($x = x_o = \alpha\lambda/2$, $z = z_o = \beta\lambda$) is thus expressed as (18), which is a function of the variables α and β, and the mode number m. As another expression of the electric field at P_o, we can obtain (19) by applying the relationships of $\alpha = L/(\lambda(1+2T))$ and $\beta = T\alpha$ to (18). In addition, we derive a geometrical limitation to the existence of an electric field with the propagation mode for $\pm z$ directions because the electric fields with the propagation mode dominantly affect the total electric field. Solving the condition of $\xi_m \geq 0$ yields (20), which is the resulting condition composed of the geometrical parameters L and T, wavelength λ, and mode number m.

$$E_y(x,z) = i\omega \sum_{m=1}^{M} A_m \sin\gamma_m x \sin\xi_m z = \omega \sum_{m=1}^{M} \frac{A_m}{2}(e^{i\xi_m z} - e^{-i\xi_m z}) \sin\gamma_m x \tag{17}$$

where $\gamma_m = m\pi/\alpha\lambda$, $\xi_m = \sqrt{k^2-\gamma_m^2} = \sqrt{(2\pi/\lambda)^2-(m\pi/\alpha\lambda)^2}$, and M and A_m are the maximum mode number and modal coefficient, respectively.

$$E_y(x=x_o, z=z_o) = i\omega \sum_{m=1}^{M} A_m \sin\frac{m\pi}{2} \sin\left(\frac{\beta\pi\sqrt{4\alpha^2-m^2}}{\alpha}\right) \tag{18}$$

$$E_y(x=x_o, z=z_o) = i\omega \sum_{m=1}^{M} A_m \sin\frac{m\pi}{2} G(T,L,m) \tag{19}$$

where $G(T,L,m) = \sin\left(\pi T\sqrt{4\left(\frac{L}{\lambda(1+2T)}\right)^2 - m^2}\right)$.

$$\frac{m}{2} < \alpha \text{ or } \frac{L}{m\lambda} - \frac{1}{2} > T. \tag{20}$$

After mathematically understanding the electric field of each mode in (19), we find that the total electric field strength at P_o is determined by the electric fields of only odd modes ($m = 1, 3, 5, \ldots$) because of $\sin m\pi/2$. In addition, we observe that the mode of a propagating electric field depends on the total length L and ratio T. For varying total length L and ratio T at 5 GHz, Fig. 7(a) shows the existing modes of propagating electric fields at P_o; Figs. 7(b), (c), and (d) show $G(T, L, m)$ corresponding to $m = 1$, 3, and 5 at P_o, respectively.

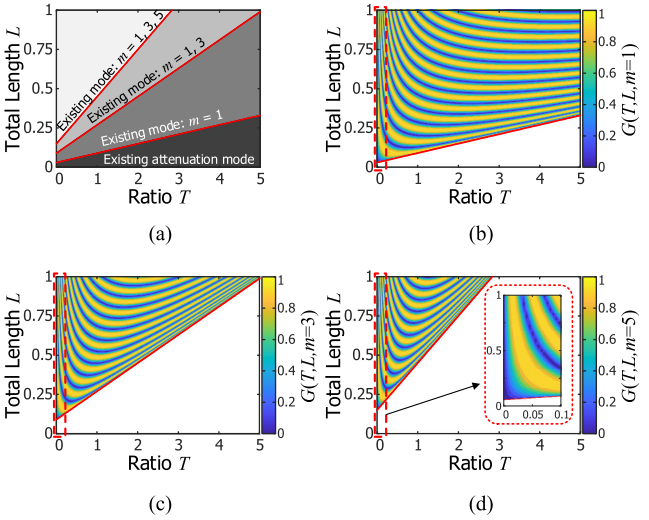

FIGURE 7. (a) Existing modes of propagating electric fields, (b) $G(T, L, m = 1)$, (c) $G(T, L, m = 3)$, and (d) $G(T, L, m = 5)$ at observation point Po while varying both ratio T and total length L at 5 GHz.

In Fig. 7(a), the maximum mode of a propagating electric field increases as either ratio T approaches zero or total length L increases. Furthermore, in Figs. 7(b), (c), and (d), $G(T, L, m)$ in each mode ($m = 1$, 3, or 5) is constant irrespective of the total length L when ratio T approaches zero (indicated by a red dashed line). These results indicate that the variation in total length L almost has no effect on the propagating electric field at P_o in cable tray II with ratio T of approximately zero ($T \approx 0$). In other words, this result implies that the lateral walls with small height do not play an important role in reducing the electric-field strength at P_o.

Note that the aforementioned EM characteristics are useful in understanding the mode-matching results in Figs. 10 (a), (b), and (c) of Section V, where the electric-field strength at P_o is not sensitive to the change of the total length L when the ratio T of cable tray II is lower than 1.

V. MODE-MATCHING RESULTS

In this section, we discuss the validation of our mode-matching analysis by introducing the convergence of the infinite series solutions for EM fields, as well as by comparing electric field distribution from our mode-matching analysis with that from a commercial EM simulator (COMSOL Multiphysics [22]) based on a finite element method (FEM). Subsequently, to derive the characteristics of the electric fields interfering with the victim cable tray, we calculated the strength of the interfering electric field in terms of the geometrical parameters such as the separation distance between cable trays I and II, configuration of cable trays (ratio T), and location of the electric line current in the frequency regime. In addition, we employed all propagation modes ($\xi \geq 0$) and

double attenuation modes ($\xi < 0$) for each region in analysis results.

A. VALIDATION OF THE MODE-MATCHING ANALYSIS

Before obtaining computed results regarding the EMI from an electric-line current, we first checked the convergence behavior of the resulting series solution for an electric field in each region. We examined the change in the relative error (η) at a specific observation point in each region corresponding to the increase in the maximum mode number ($M = h$) [17], [23]. The definition of the relative error at observation point P_n ($x = x_n, z = z_n$) in region n is

$$\eta_n = \left| \frac{E_y^n(x_n, z_n)\Big|_{M=M_n} - E_y^n(x_n, z_n)\Big|_{M=h}}{E_y^n(x_n, z_n)\Big|_{M=M_n}} \right|. \tag{21}$$

where $h = 1, 2, 3, \cdots, M_n$ for region n.

Fig. 8 shows the investigated resulting relative errors at 3 GHz when the electric-line current with 0.001 A/m^2 is located at ($x = x' = (x_3 + x_4)/2, z = z' = z_3/2$). In Fig. 8, we located the observation point in the position shifted by 0.001λ from the center point of each region because the electric fields with even modes are neglected at the central location in each region, as mentioned in Section II. For example, observation point P_1 in region I is set as ($x = (x_2 + x_3)/2 + 0.001\lambda, z = z_4/2 + 0.001\lambda$). In Fig. 8, we set the geometrical parameters as $d_1 = d_2 = h_1 = h_3 = 0.5$ m, $l_1 = l_2 = 0.09$ m, $h_2 = 0.045$ m, $t = 0.005$ m, and $a = 0.0125$ m. Fig. 8 shows that the relative error approaches 0% as the maximum mode number ($M = h$) increases in each region, thus validating the formulation and computation of our mode-matching analysis. Based on P_1 and P_2 in Fig. 8, the electric fields with mode numbers ranging from 1 to 20 have a phase difference of 180° with respect to the total electric field ($E_y^n(x_n, z_n)\Big|_{M=M_n}$), resulting in a relative error above 100%.

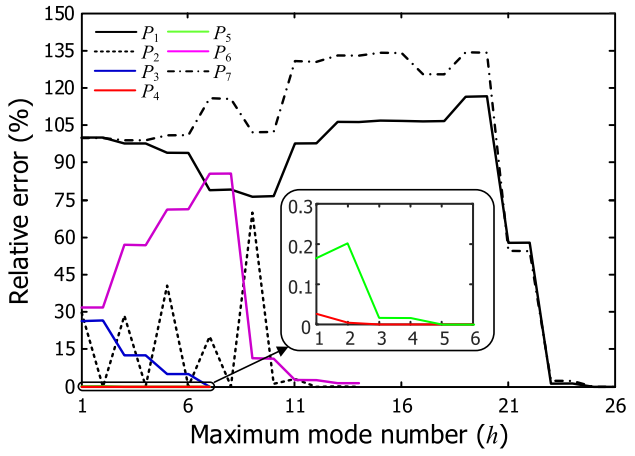

FIGURE 8. Investigated relative errors defined in (21) at a specific observation point in each region to validate the convergence behavior.

As another validation of our mode-matching analysis, we compared the electric-field distribution at 5 GHz calculated using the mode-matching method with that computed using a commercial EM simulator (COMSOL Multiphysics [22]), as shown in Fig. 9, where the geometrical parameters and the strength of the electric-line current are the same as those in Fig. 8, except that $d_1 = d_2 = h_1 = h_3 = 0.06$ m. In Figs. 9(a) and (b), the electric-field strengths and distributions computed using our mode-matching method and the commercial EM simulator show a good agreement. For a quantitative comparison, we investigated the

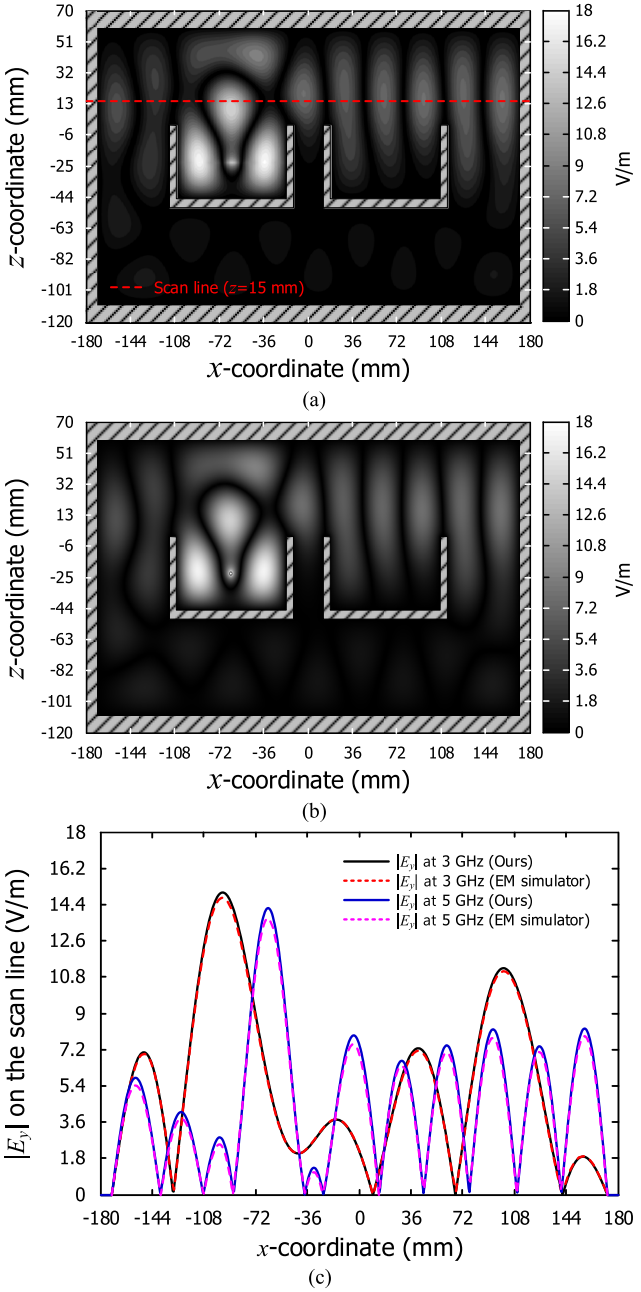

FIGURE 9. Comparison of the electric-field distributions derived by (a) a mode-matching method and (b) a commercial EM simulator; and (c) electric field strength along the scan line.

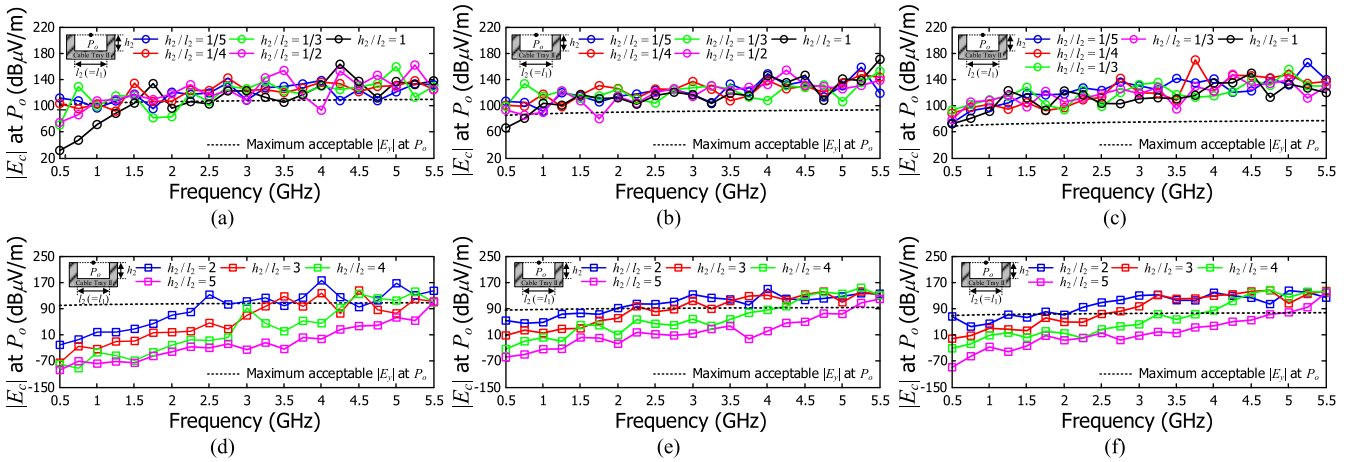

FIGURE 10. Electric-field strengths at the observation point Po in different separation distances (2a) between cable trays I and II when the ratio T ($= h_2 / l_2$) are set as 1/5, 1/4, 1/4, 1/2, 1, 2, 3, 4, and 5. The separation distance (2a) between cable trays I and II are set as 25 mm in (a) and (d), 152 mm in (b) and (e), and 920 mm in (c) and (f).

electric-field strength along the scan line (indicated by a red line in Fig. 9(a)), as shown in Fig. 9(c). Fig. 9(c) shows a good agreement between the two results. Thus, we can confirm that our mode-matching method is valid and suitable for the analysis of this EM problem.

B. EM INTERPRETATION OF CABLE TRAYS I AND II

We calculated the strength of an electric field at observation point P_o to evaluate the interference of the electric field penetrating into cable tray II. Fig. 10 represents the investigated electric-field strengths for the cases with separation distances ($2a$) of 0.025, 0.152, and 0.920 m, while the frequency changes from 0.5 GHz to 5.5 GHz and ratio T changes in total length L of 0.3 m. In Fig. 10, we set the geometrical parameters as $d_1 = d_2 = h_1 = h_3 = 5\lambda$, $t = 0.005$ m. To explain the results presented in Fig. 10 in detail, the interfering electric field at P_o increased while the frequency increased. In a comparison between the cases with a ratio T smaller than 1 (Figs. 10(a)–(c)) and the cases with ratio T larger than 1 (Figs. 10(d)–(f)), the electric-field strength at P_o is more proportional to the frequency under the cases where ratio T is larger than 1. For ratio T, Fig. 10 shows that the electric-fi eld strength at P_o increases in inverse proportion to ratio T and then is maintained constantly without any distinct increase in the investigated frequency range as ratio T steps down from 5 to 1/5. This electric-field strength, which is insensitive to the frequency for the cable tray with a small ratio T, can be understood by the previous explanation in Section II, where the electric-field strength at P_o in each mode is not sensitive to the total length in the condition that the cable tray has a small ratio T.

As another characteristic, Fig. 10 provides us with the frequency range for the electric-field strength at P_o not to exceed the allowable electric-field strength as depicted as a dash line in Section II. For example, the result for the case with a T ratio of 2 and a separation distance of 0.025 m in Fig. 10(d) indicates that such open cable trays should be used at frequencies lower than approximately 2.5 GHz. Focusing the results in the cases where the separation distances are 0.025 mm (Figs. 10(a) and (d)), 0.152 m (Figs. 10(b) and (e)), and 0.92 m (Figs. 10(c) and (f)), the electric fields at P_o in the case with a separation distance of 0.152 m are stronger than those with a separation distance of 0.025 m. Otherwise, we found no remarkable discrepancy in electric-field strength at P_o between the two cases with separation distances of 0.152 and 0.920 m, respectively. These results imply that the EM radiation and reflection more dominantly affect the interfering electric field at P_o than does the proximity EM coupling in a near field zone.

Consequently, Fig. 10 provides us useful information about the proper ratio T, adequate separation distance, and frequency range for the electric-field strength at P_o to meet the acceptance criterion for regulation.

Next, we investigated the variation in the electric-field strengths at radiating point P_r and observation point P_o while adjusting the location of the electric-line current ($x = x'$, $z = z'$) in cable tray I on the x- and z-axes. First, we represent the calculated electric-field strengths at P_r and P_o while location x' of the electric-line current at $z = z_3/2$ horizontally varies from x_3 to x_4 at 3 and 5 GHz, as shown in Fig. 11. The circular markers indicate the cases in which the electric-field strengths at P_r and P_o are either maximized or minimized. In Fig. 11, we set the geometrical parameters as $d_1 = d_2 = h_1 = h_3 = 0.06$ m ($= \lambda$ at 5 GHz), $t = 0.005$ m, $a = 0.0125$ m, $h_2 = 0.045$ m, and $l_1 = l_2 = 0.09$ m (ratio $T = 0.5$ and total length $L = 0.18$ m).

Fig. 11 shows that the electric-field strengths at P_r and P_o vary depending on location x' and the frequency. Specifically, the investigated electric-field strength at P_o in 5 GHz has a similar tendency to that at P_r overall, except for the case of location $x' = -85.4$ mm. In addition, the investigated electric-field strengths at P_r and P_o drastically decrease at locations $x' = -85.4$, -55.3, and -51.7 mm at 5 GHz, as compared with those at 3 GHz. For an in-depth study of the results presented in Fig. 11, we derived the electric-field distributions at location $x' = -85.4$, -55.3, and -36 mm,

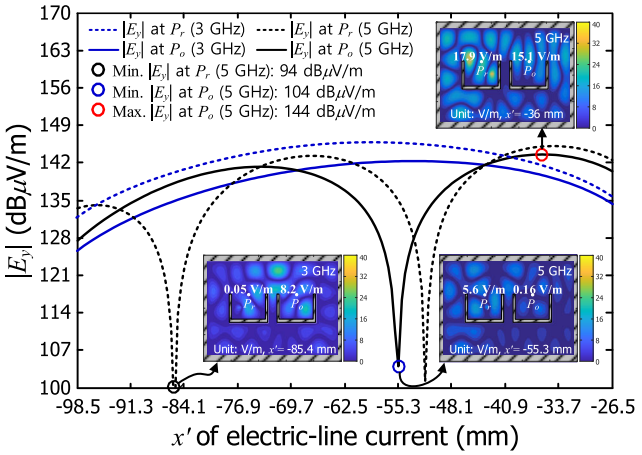

FIGURE 11. Electric-field strength at the observation point while the location of the electric-line varies along the *x*-axis at $z = -h_2/2$.

as illustrated as insets in Fig. 11. The electric-field distributions in cases of location $x' = -55.3$ and -36 mm inform that the strength of the electric field in cable tray II is proportional to the strength of the electric field generated between the electric-line current and the side walls in cable tray I. Furthermore, the electric-field distribution when $x' = -85.4$ mm also shows that the electric field in cable tray II can be stronger owing to the reflection of a ceiling even though the electric field in cable tray I is weak. These results imply that not only the geometrical parameters of cable trays but also the distance from a ceiling should be considered in the installation of cable trays in a nuclear power plant.

In addition, we investigated the variation in the strength of electric fields at P_r and P_o in 5 GHz, while location z' of the electric-line current at $x = (x_3 + x_4)/2$ vertically varies from z_3 toward zero as shown in Fig. 12. In Fig. 12, we appended the overall electric-field distributions for cases in which the electric-field strengths at P_r and P_o are either maximized or minimized as marked with circles. The electric-field strength at P_r is maximum at $z' = -29.3$ mm (depicted as a red circular marker) and then drastically decreases at $z' = -14$ mm (as illustrated by a blue circular marker). The investigated

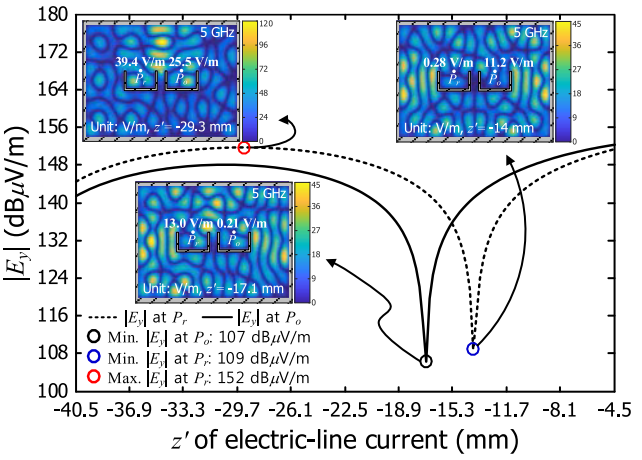

FIGURE 12. Electric-field strength at observation point while the location of the electric-line varies along the *z*-axis at 5 GHz.

electric-field strength at P_o is similar to the electric-field strength P_r, as shown in Fig. 12. We revealed that the electric field reflected from the bottom plate of cable tray I makes the electric field at P_r either strong or weak. This is because the reflected electric field is in phase when $z' = -29.3$ mm (0.26λ apart from the bottom plate at 5 GHz) and out of phase when $z' = -14$ mm (0.52λ apart from the bottom plate at 5 GHz).

Note that we can expect this result on the basis of the previous explanation in Section IV, where we approximately examined the electric field reflected from the bottom plate of cable tray I using image theory.

VI. CONCLUSION

This paper presents an analytical interpretation of the electromagnetic interference between open cable trays of solid-bottom type in a nuclear power plant, under the assumption that an electric-line current is undesirably generated from a damaged cable in an open cable tray. We investigated the regulatory guidance on electrical independence of cable trays in terms of various placements of both open and enclosed cable trays, and regulatory requirements to avoid electromagnetic interference between open cable trays in a nuclear power plant. Then, we applied the mode-matching method to the electromagnetic analysis of two open cable trays installed in an indoor environment to alleviate the electromagnetic interference. Specifically, in the mode-matching method, we used both the superposition principle and Helmholtz equation in conjunction with the separation of variables to express the electromagnetic field. The boundary conditions for the tangential electric- and magnetic-field continuities between the separated regions were enforced to obtain the modal coefficients in each region.

Before obtaining the modal coefficients from a set of simultaneous equations, we performed an approximate estimation of the interfering electric field between the open cable trays by deriving an array factor in conjunction with image theory and analyzing an interfering electric field in an individual mode. We then derived modal coefficients by enforcing boundary conditions and validated the mode-matching analysis by checking the convergence of a mode-matching solution and comparing the mode-matching result with commercial simulation. Next, we evaluated the electric fields interfering with a victim cable tray using computed modal coefficients while varying the geometrical parameters such as the configuration of the cable tray and the location of an electric line current. From the investigated electric-field strength and distributions, we extracted effective geometrical parameters to control and mitigate the interfering electric field. We expect that the analysis method proposed in this paper can be utilized practically as a precautionary measure against electromagnetic interference in actual nuclear power plant environments.

APPENDIX

In this section, we describe the boundary conditions on the continuities of the tangential electric and magnetic fields,

applied to obtain a set of simultaneous equations, which determine the unknown modal coefficients. We substitute the expressions of the electric and magnetic fields into the boundary conditions. We then utilize the orthogonality of the sinusoidal functions by multiplying a sinusoidal function and integrating it with respect to x for each boundary condition. Herein, we additionally show the boundary conditions at $z = z_2$, explain the boundary conditions (9) and (10) in detail, and describe the matrix equations from simultaneous equations

A. BOUNDARY CONDITIONS AT $Z = Z_2$

The boundary condition on the continuity of the tangential electric field at $z = z_2$ is expressed as follow.

$$E_y^{VII}(x,z)\Big|_{z=z_2} = \begin{cases} E_y^{II}(x,z)\Big|_{z=z_2}, & x_1 \le x < x_2 \\ 0, & x_2 \le x < x_5 \\ E_y^{IV}(x,z)\Big|_{z=z_2}, & x_5 \le x < x_6 \\ 0, & x_6 \le x < x_9 \\ E_y^{VI}(x,z)\Big|_{z=z_2}, & x_9 \le x < x_{10} \end{cases} \tag{A1}$$

The boundary conditions on the continuity of the tangential magnetic field at $z = z_2$ are expressed as follow.

$$H_x^{VII}(x,z)\Big|_{z=z_2} = H_x^{II}(x,z)\Big|_{z=z_2}, \quad x_1 < x < x_2 \tag{A2}$$

$$H_x^{VII}(x,z)\Big|_{z=z_2} = H_x^{IV}(x,z)\Big|_{z=z_2}, \quad x_5 < x < x_6 \tag{A3}$$

$$H_x^{VII}(x,z)\Big|_{z=z_2} = H_x^{VI}(x,z)\Big|_{z=z_2}, \quad x_9 < x < x_{10} \tag{A4}$$

B. BOUNDARY CONDITION ON THE CONTINUITY OF THE TANGENTIAL ELECTRIC FIELD

For the boundary condition (9) on the continuity of the tangential electric field at $z = 0$, we substitute (1)−(7) for regions I–VI into (9). We then multiply the resulting (9) by $\sin\gamma_{p_1}(x - x_1)$ and integrate the result with respect to x from x_1 to x_{10} $\left(\int_{x_1}^{x_{10}} (\cdot)\sin\gamma_{p_1}(x - x_1)dx\right)$, yielding

$$\begin{aligned} &\sum_{m_1=1}^{M_1} A_{m_1}\frac{x_1 - x_{10}}{2}\delta_{m_1p_1}\sin\xi_{m_1}z_4 \\ &\quad - \sum_{m_2=1}^{M_2} B_{m_2}F(x_1,x_2,x_1,\gamma_{m_2},\gamma_{p_1}) \\ &\quad + \sum_{m_3=1}^{M_3} A_{m_3}F(x_3,x_4,x_1,\gamma_{m_3},\gamma_{p_1})\sin\xi_{m_3}z_3 \\ &\quad - \sum_{m_4=1}^{M_4} B_{m_4}F(x_5,x_6,x_1,\gamma_{m_4},\gamma_{p_1}) \\ &\quad + \sum_{m_5=1}^{M_5} A_{m_5}F(x_7,x_8,x_1,\gamma_{m_5},\gamma_{p_1})\sin\xi_{m_5}z_3 \\ &\quad - \sum_{m_6=1}^{M_6} B_{m_6}F(x_9,x_{10},x_1,\gamma_{m_6},\gamma_{p_1}) = 0, \end{aligned} \tag{A5}$$

where $\delta_{mn} = \begin{cases} 1, & if\ m = n \\ 0, & otherwise \end{cases}$ and

$$F(a,b,c,m,p) = \int_a^b \sin m(x-a)\sin p(x-c)dx.$$

C. BOUNDARY CONDITION ON THE CONTINUITY OF THE TANGENTIAL MAGNETIC FIELD

For the boundary condition (10) on the continuity of the tangential magnetic field at $z = 0$ in the range of $x_1 < x < x_2$, we derive the tangential magnetic fields by applying the relationship of $H_x = (i/\omega\mu)\cdot(dE_y/dz)$ to (2)−(3) as follows.

$$\begin{aligned} H_x^{II}(x,z) &= \frac{i}{\omega\mu}\frac{dE_y^{II}(x,z)}{dz} \\ &= -\sum_{m_2=1}^{M_2}\frac{\xi_{m_2}}{\mu}\sin\gamma_{m_2}(x-x_1) \\ &\quad \times (A_{m_2}\cos\xi_{m_2}z - B_{m_2}\sin\xi_{m_2}z) \end{aligned} \tag{A6}$$

$$\begin{aligned} H_x^{III}(x,z) &= \frac{i}{\omega\mu}\frac{dE_y^{III}(x,z)}{dz} \\ &= -\sum_{m_3=1}^{M_3}\frac{\xi_{m_3}}{\mu}A_{m_3}\sin\gamma_{m_3}(x-x_3)\cos\xi_{m_3}(z-z_3) \end{aligned} \tag{A7}$$

We then multiply the resulting (10) by $\sin\gamma_{p_2}(x - x_1)$ and integrate the result with respect to x from x_1 to x_2 $\left(\int_{x_1}^{x_2} (\cdot)\sin\gamma_{p_2}(x - x_1)dx\right)$, yielding

$$\begin{aligned} &\sum_{m_1=1}^{M_1} A_{m_1}\xi_{m_1}F(x_1,x_2,x_1,\gamma_{p_2},\gamma_{m_1})\cos\xi_{m_1}z_4 \\ &\quad - \sum_{m_2=1}^{M_2} A_{m_2}\xi_{m_2}\frac{x_2 - x_1}{2}\delta_{m_2p_2} = 0. \end{aligned} \tag{A8}$$

Similarly, the other simultaneous equations from the boundary conditions on the continuities (11), (12) and (A1)−(A4) are derive as (A9)−(A16), respectively.

$$\begin{aligned} &\sum_{m_1=1}^{M_1} A_{m_1}\xi_{m_1}F(x_3,x_4,x_1,\gamma_{p_3}\gamma_{m_1})\cos\xi_{m_1}z_4 \\ &\quad - \sum_{m_3=1}^{M_3} A_{m_3}\xi_{m_3}\frac{x_4 - x_3}{2}\delta_{m_3p_3}\cos\xi_{m_3}z_3 \\ &= -\sum_{m_3=1}^{M_3}\frac{J(x_4 - x_3)\sin\gamma_{m_3}(x' - x_3)\sin\xi_{m_3}(z' - z_3)}{l_1\sin\xi_{m_3}h_2}\delta_{m_3p_3} \end{aligned} \tag{A9}$$

$$\begin{aligned} &\sum_{m_1=1}^{M_1} A_{m_1}\xi_{m_1}F(x_5,x_6,x_1,\gamma_{p_4},\gamma_{m_1})\cos\xi_{m_1}z_4 \\ &\quad - \sum_{m_4=1}^{M_4} A_{m_4}\xi_{m_4}\frac{x_6 - x_5}{2}\delta_{m_4p_4} = 0 \end{aligned} \tag{A10}$$

$$\sum_{m_1=1}^{M_1} A_{m_1}\xi_{m_1}F(x_7, x_8, x_1, \gamma_{p_5}, \gamma_{m_1})\cos\xi_{m_1}z_4 - \sum_{m_5=1}^{M_5} A_{m_5}\xi_{m_5}\frac{x_8 - x_7}{2}\delta_{m_5p_5}\cos\xi_{m_5}z_3 = 0 \quad \text{(A11)}$$

$$\sum_{m_1=1}^{M_1} A_{m_1}\xi_{m_1}F(x_9, x_{10}, x_1, \gamma_{p_6}, \gamma_{m_1})\cos\xi_{m_1}z_4 - \sum_{m_6=1}^{M_6} A_{m_6}\xi_{m_6}\frac{x_{10} - x_9}{2}\delta_{m_6p_6} = 0 \quad \text{(A12)}$$

$$\sum_{m_2=1}^{M_2} A_{m_2}F(x_1, x_2, x_1, \gamma_{m_2}, \gamma_{p_7})\sin\xi_{m_2}z_2 + \sum_{m_2=1}^{M_2} B_{m_2}F(x_1, x_2, x_1, \gamma_{m_2}, \gamma_{p_7})\cos\xi_{m_2}z_2 + \sum_{m_4=1}^{M_4} A_{m_4}F(x_5, x_6, x_1, \gamma_{m_4}, \gamma_{p_7})\sin\xi_{m_4}z_2 + \sum_{m_4=1}^{M_4} B_{m_4}F(x_5, x_6, x_1, \gamma_{m_4}, \gamma_{p_7})\cos\xi_{m_4}z_2 + \sum_{m_6=1}^{M_6} A_{m_6}F(x_9, x_{10}, x_1, \gamma_{m_6}, \gamma_{p_7})\sin\xi_{m_6}z_2 + \sum_{m_6=1}^{M_6} B_{m_6}F(x_9, x_{10}, x_1, \gamma_{m_6}, \gamma_{p_7})\cos\xi_{m_6}z_2 - \sum_{m_7=1}^{M_7} A_{m_7}\frac{x_{10} - x_1}{2}\delta_{m_7p_7}\sin\xi_{m_7}(z_2 - z_1) = 0 \quad \text{(A13)}$$

$$\sum_{m_2=1}^{M_2} A_{m_2}\xi_{m_2}\frac{x_2 - x_1}{2}\delta_{m_2p_2}\cos\xi_{m_2}z_2 - \sum_{m_2=1}^{M_2} B_{m_2}\xi_{m_2}\frac{x_2 - x_1}{2}\delta_{m_2p_2}\sin\xi_{m_2}z_2 - \sum_{m_7=1}^{M_7} A_{m_7}\xi_{m_7}F(x_1,x_2,x_1,\gamma_{p_2},\gamma_{m_7})\cos\xi_{m_7}(z_2-z_1)=0 \quad \text{(A14)}$$

$$\sum_{m_4=1}^{M_4} A_{m_4}\xi_{m_4}\frac{x_6 - x_5}{2}\delta_{m_4p_4}\cos\xi_{m_4}z_2 - \sum_{m_4=1}^{M_4} B_{m_4}\xi_{m_4}\frac{x_6 - x_5}{2}\delta_{m_4p_4}\sin\xi_{m_4}z_2 - \sum_{m_7=1}^{M_7} A_{m_7}\xi_{m_7}F(x_5,x_6,x_1,\gamma_{p_4},\gamma_{m_7})\cos\xi_{m_7}(z_2-z_1)=0 \quad \text{(A15)}$$

$$\sum_{m_6=1}^{M_6} A_{m_6}\xi_{m_6}\frac{x_{10} - x_9}{2}\delta_{m_6p_6}\cos\xi_{m_6}z_2 - \sum_{m_6=1}^{M_6} B_{m_6}\xi_{m_6}\frac{x_{10} - x_9}{2}\delta_{m_6p_6}\sin\xi_{m_6}z_2 - \sum_{m_7=1}^{M_7} A_{m_7}\xi_{m_7}F(x_9,x_{10},x_1,\gamma_{p_6},\gamma_{m_7})\cos\xi_{m_7}(z_2-z_1)=0 \quad \text{(A16)}$$

D. MATRIX EQUATION

The simultaneous equations from the enforcement of the boundary conditions can be expressed as a matrix equation for the modal coefficients $A_{m_1}, A_{m_2}, A_{m_3}, A_{m_4}, A_{m_5}, A_{m_6}, A_{m_7}$, B_{m_2}, B_{m_4}, and B_{m_6} as follows.

$$\begin{bmatrix} \varphi_{1,1} & 0 & \varphi_{1,3} & \varphi_{1,4} & 0 & \varphi_{1,6} & \varphi_{1,7} & 0 & \varphi_{1,9} & 0 \\ \varphi_{2,1} & \varphi_{2,2} & 0 & 0 & 0 & 0 & 0 & 0 & 0 & 0 \\ \varphi_{3,1} & 0 & 0 & \varphi_{34} & 0 & 0 & 0 & 0 & 0 & 0 \\ \varphi_{4,1} & 0 & 0 & 0 & \varphi_{4,5} & 0 & 0 & 0 & 0 & 0 \\ \varphi_{5,1} & 0 & 0 & 0 & 0 & 0 & \varphi_{5,7} & 0 & 0 & 0 \\ \varphi_{6,1} & 0 & 0 & 0 & 0 & 0 & 0 & \varphi_{6,8} & 0 & 0 \\ 0 & \varphi_{7,2} & \varphi_{7,3} & 0 & \varphi_{7,5} & \varphi_{7,6} & 0 & \varphi_{7,8} & \varphi_{7,9} & \varphi_{7,10} \\ 0 & \varphi_{8,2} & \varphi_{8,3} & 0 & 0 & 0 & 0 & 0 & 0 & \varphi_{8,10} \\ 0 & 0 & 0 & 0 & \varphi_{9,5} & \varphi_{9,6} & 0 & 0 & 0 & \varphi_{9,10} \\ 0 & 0 & 0 & 0 & 0 & 0 & 0 & \varphi_{10,8} & \varphi_{10,9} & \varphi_{10,10} \end{bmatrix} \begin{bmatrix} C_1 \\ C_2 \\ C_3 \\ C_4 \\ C_5 \\ C_6 \\ C_7 \\ C_8 \\ C_9 \\ C_{10} \end{bmatrix} = \begin{bmatrix} 0 \\ 0 \\ S_3 \\ 0 \\ 0 \\ 0 \\ 0 \\ 0 \\ 0 \\ 0 \end{bmatrix}$$

where $\boldsymbol{C_1}, \boldsymbol{C_2}, \boldsymbol{C_3}, \boldsymbol{C_4}, \boldsymbol{C_5}, \boldsymbol{C_6}, \boldsymbol{C_7}, \boldsymbol{C_8}, \boldsymbol{C_9}, \boldsymbol{C_{10}}$, are column vectors consisting of elements $A_{m_1}, A_{m_2}, B_{m_2}, A_{m_3}, A_{m_4}, B_{m_4}, A_{m_5}, A_{m_6}$, B_{m_6}, A_{m_7}, respectively. The elements of vectors $\boldsymbol{\varphi}$ and $\boldsymbol{S}$ in the above matrix equation are derived from equations (A5) and (A8)−(A16). For example, the elements of $\boldsymbol{\varphi_{3,1}}$, $\boldsymbol{\varphi_{3,4}}$, and $\boldsymbol{S_3}$ corresponding to the mode numbers m_1 and m_3 are obtained from (A9), as follow.

$\varphi_{2,1}=\xi_{m_1}F(x_3, x_4, x_1, \gamma_{p_3}, \gamma_{m_1})\cos\xi_{m_1}z_4$ for m_1

$\varphi_{3,4} = 0.5\xi_{m_3}(x_3 - x_4,)\delta_{m_3p_3}\cos\xi_{m_3}z_3$ for m_3

$S_3 = J(x_3 - x_4)\sin\gamma_{m_3}(x' - x_3)\sin\xi_{m_3}(z' - z_3)\delta_{m_3p_3}/(l_1\sin\xi_{m_3}h_2)$ for m_3

REFERENCES

[1] *Chalfant Manufacturing Company*. Accessed: May 20, 2019. [Online]. Available: https://www.chalfant-obo.com

[2] A. W. Scheide, "Evaluation of the shielding properties of cable trays for use in an industrial environment," *IEEE Trans. Ind. Appl.*, vol. IA-8, no. 6, pp. 783–787, Nov. 1972.

[3] S. Kapora, E. Laermans, and A. P. J. van Deursen, "Protection of cables by open-metal conduits," *IEEE Trans. Electromagn. Compat.*, vol. 52, no. 4, pp. 1026–1033, Nov. 2010.

[4] D. Zhang, Y. Wen, Y. Wang, D. Liu, X. He, and J. Fan, "Coupling analysis for wires in a cable tray using circuit extraction based on mixed-potential integral equation formulation," *IEEE Trans. Electromagn. Compat.*, vol. 59, no. 3, pp. 862–872, Jun. 2017.

[5] W. L. de Souza, H. de Paula, A. De Conti, and R. C. Mesquita, "Cable parameter calculation for typical industrial installation methods and high-frequency studies," *IEEE Trans. Ind. Appl.*, vol. 54, no. 4, pp. 3919–3927, Jul./Aug. 2018.

[6] M. J. A. M. van Helvoort, "Grounding structures for the EMC-protection of cabling and wiring," Ph.D. dissertation, Dept. Elect. Eng., Eindhoven Univ. Technol., Eindhoven, The Netherlands, 1995.

[7] A. P. J. van Deursen, "Schwarz-Christoffel analysis of cable conduits with noncontacting cover," *Electron. Lett.*, vol. 37, no. 13, pp. 816–817, 2001.

[8] A. P. J. van Deursen, F. B. M. van Horck, M. J. A. M. van Helvoort, and P. C. T. van der Laan, "Transfer impedance of nonmagnetic conduits of various shapes," *IEEE Trans. Electromagn. Compat.*, vol. 43, no. 1, pp. 18–28, Feb. 2001.

[9] N. W. Ebertsohn, R. H. Geschke, and H. C. Reader, "Cable trays in EMC: Measurement and modeling to 30 MHz," *IEEE Trans. Electromagn. Compat.*, vol. 49, no. 2, pp. 346–353, May 2007.

[10] P. S. van der Merwe, H. C. Reader, and D. J. Rossouw, "Cable tray connections for electromagnetic interference (EMI) mitigation," *IEEE Trans. Electromagn. Compat.*, vol. 53, no. 2, pp. 332–338, May 2011.

[11] *Guideline for Evaluating Electromagnetic and Radio-Frequency Interference in Safety-Related Instrumentation and Control Systems, Regulatory Guide 1.180*, Nucl. Regulatory Commision, U.S. Dept. Energy, Washington, DC, USA, Oct. 2003.
[12] *Criteria for Independence of Electrical Safety Systems*, Regulatory Guide 1.75, U.S. Nucl. Regulatory Commission, U. S. Dept. Energy, Washington, DC, USA, Feb. 2005.
[13] *IEEE Standard Criteria for Independence of Class 1E Equipment and circuits*, IEEE Standard 384, Dec. 2008.
[14] *Requirements for the Control of Electromagnetic Interference Characteristics of Subsystems and Equipment*, Standard Mil-Std-461E, U. S. Dept. Defense, Washington, DC, USA, Aug. 1999.
[15] H. J. Eom, *Wave Scattering Theory*. Berlin, Germany: Springer Verlag, 2001.
[16] D. I. Yang, H. J. Eom, and J. W. Ra, "Radiation from groove-backed antennas with a gap," *IEEE Antennas Wireless Propag. Lett.*, vol. 3, pp. 208–210, Jul. 2004.
[17] J. Choo, J.-E. Park, H. Choo, and Y.-H. Kim, "Electromagnetic interference caused by parasitic electric-line current on a digital module in a closed cabinet," *IEEE Access*, vol. 7, pp. 59806–59812, May 2019.
[18] J. Choo, J. Choo, and Y.-H. Kim, "Shielding effectiveness of open cabinet containing digital modules using ferrite sheet," *IEEE Trans. Magn.*, vol. 53, no. 12, pp. 1–9, Dec. 2017.
[19] C. A. Balanis, *Antenna Theory: Analysis and Design*, 4th ed. New York, NY, USA: Wiley, 2016, ch. 4, sec. 7, pp. 179–203.
[20] J. D. Kraus and R. J. Marhefka, *Antennas for All Applications*, 3rd ed. New York, NY, USA: McGraw-Hill, 2002, ch. 10, sec. 2, pp. 349–352.
[21] W. L. Stutzman and G. A. Thiele, *Antenna Theory and Design*, 3rd ed. New York, NY, USA: Wiley, 2012, ch. 8, sec. 2, pp. 272–278.
[22] *COMSOL Multiphysics 5.4*. Accessed: Jan. 1, 2020. [Online]. Available: https://www.comsol.com
[23] J. Choo, J. Choo, and Y.-H. Kim, "Evaluation of electromagnetic interference from axially ruptured coaxial cable with multiple dielectrics used in nuclear power plants," *IEEE Trans. Electromagn. Compat.*, vol. 61, no. 3, pp. 860–869, Jun. 2019.

JAEYUL CHOO received the B.S. and M.S. degrees in electronic and electrical engineering from Hongik University, Seoul, South Korea, in 2004 and 2006, respectively, and the Ph.D. degree in electrical engineering from the Korea Advanced Institute of Science and Technology (KAIST), Daejeon, South Korea, in 2014. He was an Associate Research Engineer with the Central Research and Development Center, LS Industrial Systems Company, Ltd., Anyang, South Korea, from 2006 to 2010. In 2014, he joined the Korea Institute of Nuclear Safety, Daejeon. His current research interests include the design of tag and reader antennas for RFID, the electrical analysis for flip-chip bonding package, and the electromagnetic field analyses of vias, transmission lines, and scattering structure for dealing with electromagnetic interference problems.

HOON-KEUN LEE received the Ph.D. degree from the Department of Electrical Engineering, Korea Advanced Institute of Science and Technology (KAIST), Daejeon, South Korea, in 2014. He is currently working with the Korea Institute of Nuclear Safety (KINS), as a Senior Researcher. His research interests include optical fiber sensors, optical communications, and digital I&C systems.

JONG-EON PARK received the B.S., M.S., and Ph.D. degrees from the School of Electrical Engineering and Computer Science, Kyungpook National University, Daegu, South Korea, in 2006, 2009, and 2013, respectively. From 2013 to 2015, he was a Postdoctoral Researcher with The Ohio State University. From 2016 to 2019, he was a Research Professor with Hongik University. Since 2020, he has been with Dongguk University, where he is currently an Assistant Professor with the Department of Safety Engineering. His research interests include scattering through aperture, antenna design, and computational electromagnetics.

HOSUNG CHOO received the B.S. degree in radio science and engineering from Hanyang University, Seoul, South Korea, in 1998, and the M.S. and Ph.D. degrees in electrical and computer engineering from The University of Texas at Austin, in 2000 and 2003, respectively. In September 2003, he joined the School of Electronic and Electrical Engineering, Hongik University, Seoul, where he is currently a Professor. His principal area of research includes electrically small antennas for wireless communications, reader and tag antennas for RFID, on-glass and conformal antennas for vehicles and aircraft, and array antennas for GPS applications.

YONG-HWA KIM received the B.S. degree in electrical engineering and the Ph.D. degree in electrical and computer engineering from Seoul National University, Seoul, South Korea, in 2001 and 2007, respectively. From 2007 to 2011, he was a Senior Researcher with the Korea Electrotechnology Research Institute (KERI), Gyeonggi, South Korea. From 2011 to 2013, he was an Assistant Professor with the Division of Maritime Electronic and Communication Engineering, Mokpo National Maritime University, South Korea. Since March 2013, he has joined as a Faculty Member with the Department of Electronic Engineering, Myongji University, South Korea. His general research interests include communication systems, fault diagnosis, and digital signal processing. His current research interests include communications and artificial intelligence for smart grid.